Characterization of metabolites in infiltrating gliomas using *ex vivo* 1H high-resolution magic angle spinning spectroscopy

Adam Elkhaled[a,b], Llewellyn Jalbert[a,b], Alexandra Constantin[b,c], Hikari A. I. Yoshihara[b,d], Joanna J. Phillips[e,f], Annette M. Molinaro[f,g], Susan M. Chang[f] and Sarah J. Nelson[b,h]*

Gliomas are routinely graded according to histopathological criteria established by the World Health Organization. Although this classification can be used to understand some of the variance in the clinical outcome of patients, there is still substantial heterogeneity within and between lesions of the same grade. This study evaluated image-guided tissue samples acquired from a large cohort of patients presenting with either new or recurrent gliomas of grades II–IV using *ex vivo* proton high-resolution magic angle spinning spectroscopy. The quantification of metabolite levels revealed several discrete profiles associated with primary glioma subtypes, as well as secondary subtypes that had undergone transformation to a higher grade at the time of recurrence. Statistical modeling further demonstrated that these metabolomic profiles could be differentially classified with respect to pathological grading and inter-grade conversions. Importantly, the myo-inositol to total choline index allowed for a separation of recurrent low-grade gliomas on different pathological trajectories, the heightened ratio of phosphocholine to glycerophosphocholine uniformly characterized several forms of glioblastoma multiforme, and the onco-metabolite D-2-hydroxyglutarate was shown to help distinguish secondary from primary grade IV glioma, as well as grade II and III from grade IV glioma. These data provide evidence that metabolite levels are of interest in the assessment of both intra-grade and intra-lesional malignancy. Such information could be used to enhance the diagnostic specificity of *in vivo* spectroscopy and to aid in the selection of the most appropriate therapy for individual patients. © 2014 The Authors. *NMR in Biomedicine* published by John Wiley & Sons, Ltd.

Keywords: glioma; malignant transformation; 1H HR-MAS spectroscopy; metabolite profiling; 2-hydroxyglutarate; image-guided biopsy

* Correspondence to: S. J. Nelson, UCSF Mission Bay, 1700 4th St., San Francisco, CA 94158, USA.
  E-mail: Sarah.Nelson@ucsf.edu

a A. Elkhaled, L. Jalbert
  University of California, Berkeley and University of California, San Francisco Graduate Program in Bioengineering, University of California, Berkeley/San Francisco, CA, USA

b A. Elkhaled, L. Jalbert, A. Constantin, H. A. I. Yoshihara, S. J. Nelson
  Department of Radiology and Biomedical Imaging, University of California-San Francisco (UCSF), CA, USA

c A. Constantin
  National Institutes of Health, Bethesda, MD, USA

d H. A. I. Yoshihara
  Department of Cardiology, University Hospital of Lausanne (CHUV), Lausanne, Switzerland

e J. J. Phillips
  Department of Pathology, University of California-San Francisco (UCSF), CA, USA

f J. J. Phillips, A. M. Molinaro, S. M. Chang
  Department of Neurological Surgery, University of California-San Francisco (UCSF), CA, USA

g A. M. Molinaro
  Department of Biostatistics and Epidemiology, University of California, San Francisco (UCSF), CA, USA

S. J. Nelson
Department of Bioengineering and Therapeutic Sciences, University of California-San Francisco (UCSF), CA, USA

INTRODUCTION

Gliomas are tumors of the central nervous system that are routinely graded on a scale of I to IV according to histopathological criteria developed by the World Health Organization (WHO) (1,2). Whereas grade I gliomas are considered to be benign and can typically be treated through surgical intervention, infiltrating gliomas of grades II–IV present a number of challenges in making an accurate diagnosis and in selecting the most appropriate therapy. Some of the complications associated with the management of infiltrating gliomas stem from the fact that individual lesions are spatially heterogeneous and small tissue samples obtained during biopsy or surgery may not represent the most malignant region of the tumor. This situation is accentuated following treatment, where a differential response to therapy and tumor progression can cause additional ambiguity. Because clinical outcomes for glioma can be quite variable, it is important to provide criteria to more accurately assess the characteristics that change both within and between pathological grades. A further complication is that grade II and III gliomas often undergo malignant transformation at the time of recurrence, which may necessitate more aggressive therapy (3–6). This raises the question of whether individual gliomas develop *de novo* (primary glioma) at a given grade or arise as a result of transformation from a less malignant lesion (secondary glioma) that was not detected previously. As lesions of the same histological grade may arise by different mechanisms, the designation of primary and secondary glioma may have important clinical consequences for the optimization of treatment (7).

Recent findings have indicated that the metabolite characteristics of the lesion are valuable for the investigation of underlying differences in malignancy. *In vivo* metabolite imaging provides a unique opportunity for the evaluation of spatial and temporal changes in the lesion and surrounding tissue that can be used to direct tissue sampling at the time of resection, as well as for the selection and monitoring of therapy. The lesion-wide data obtained using this approach are synergistic with recent results from genome-wide sequencing and informatics-driven analyses that identify different subtypes of glioma with genetic characteristics. The ability to infer the mutational status of *isocitrate dehydrogenase* (*IDH*) genes through non-invasive MRSI of D-2-hydroxyglutarate (2HG) is an example with strong prognostic implications. This is a significant breakthrough in the realm of cancer diagnostics (8,9), because it indicates that the evaluation of new therapies that target the *IDH* pathway could be achieved non-invasively (10–13).

The primary goal of this study was to use the NMR technique of proton high-resolution magic angle spinning (^{1}H HR-MAS) spectroscopy to characterize the *ex vivo* metabolite profiles of pathologically distinct glioma subtypes at the time of initial diagnosis and at subsequent transformation. By collecting a large cohort of image-guided tissue samples, we sought to evaluate the hypothesis that different glioma subtypes have characteristic metabolite profiles that can aid in the prediction of the malignant potential. The information obtained may be used directly for improved categorization of *ex vivo* tissue samples, or can be translated into an *in vivo* setting to provide non-invasive metabolite imaging methods to direct tissue sampling, to monitor therapy and to make informed decisions about the effectiveness of different treatment strategies.

MATERIALS AND METHODS

Patient population

Our institutionally approved study comprised 126 patients receiving surgical resection as a result of suspected new or recurrent WHO grade II, III or IV glioma, who provided informed consent for image-guided tissue samples to be taken from areas designated for resection on the basis of clinical criteria. The diagnosis of grade was subsequently confirmed by a single pathologist on the basis of standard histological criteria (Table 1).

Pre-operative MRI and MRS

Pre-operative MR examinations were conducted using either 1.5- or 3-T whole-body MR scanners (GE Healthcare Technologies, Milwaukee, Wisconsin, USA) with an eight-channel, phased-array head coil for signal reception (MRI Devices, Knaresborough, United Kingdom). The data obtained included three-dimensional T_1-weighted and T_2-weighted anatomic images, six-directional diffusion-weighted imaging acquired in the axial plane (TR/TE = 1000/108 ms; voxel size, $1.7 \times 1.7 \times 3$ mm^3; $b = 1000$ s/mm^2) and, in some cases, lactate (Lac)-edited three-dimensional ^{1}H MRSI. The latter applied point-resolved spectroscopic selection (PRESS) for volume localization and very selective saturation (VSS) pulses for lipid (Lip) signal suppression (excited volume, ~$80 \times 80 \times 40$ mm^3; overpress factor, 1.5; TR/TE = 1104/144 ms; field of view, $16 \times 16 \times 16$ cm^3; nominal voxel size, $1 \times 1 \times 1$ cm^3; flyback echo-planar readout gradient in the superior-inferior direction; 712 dwell points; sweep width, 988 Hz) (14). Assessment of breakdown of the blood–brain barrier was made by administering a standard dose of Gd-DTPA (gadopentetate dimeglumine; Magnevist) prior to the acquisition of T_1-weighted inversion recovery spoiled-gradient echo (IRSPGR) images (TR/TE = 8.9/2.5 ms).

Post-processing of pre-operative MR examination

In vivo data from the pre-operative examination were transferred to a Sun Ultra 10 workstation (Sun Microsystems, Santa Clara, California, USA) and in-house software was applied to derive

Table 1. Patient population. Patients and tissue samples were stratified according to original World Health Organization (WHO) grade and recurrence status

Original WHO grade	Total	Newly diagnosed	Recurrent
	Number of patients (tissue samples)	Number of patients (tissue samples)	Number of patients (tissue samples)
II	54 (114)	0 (0)	54 (114)
III	22 (39)	5 (7)	17 (32)
IV	50 (101)	35 (70)	15 (31)
Total	126 (254)	40 (77)	86 (177)

estimates of diffusion and spectroscopic parameters. Maps of the apparent diffusion coefficient (ADC) were generated on a pixel-by-pixel basis (15). The ^{1}H MRSI data were processed in order to quantify total choline (tCho) and *N*-acetylaspartate (NAA) levels, from which maps of the choline to NAA index (CNI) could be derived. The CNI values were generated from an iterative linear regression-based algorithm that sequentially removes outlying values (16), and represent changes in choline and NAA levels relative to the normal voxels from the same subject.

Image-guided tissue sampling

The acquisition of pre-surgical *in vivo* MR data enabled the locations for tissue sampling from individual lesions to be planned prior to resection. Targets were selected from within the anatomical lesion (gadolinium-enhancing region and/or area of hyperintensity on T_2-weighted images) that demonstrated an ADC value of less than 1.5 times the value in normal-appearing white matter and/or had elevated CNI values (CNI > 3.0) from ^{1}H MRSI. Figure 1 depicts the selection of targets for a patient with a grade IV glioma. The CNI map highlights the relative elevation of choline species and reduction in NAA, which are consistent with malignant tissue. Two primary targets were defined, with one showing a local CNI maximum and the other corresponding to a region of hypointensity on the ADC map. Targets were designated from each patient as spherical regions of interest with a diameter of 5 mm on co-registered MR images using BrainLAB surgical navigation software (BrainLAB Inc., Munich, Germany). Image-guided naviga-

tion was applied to locate tissue corresponding to predefined targets, and the neurosurgeon provided samples from as close as possible to the target. The actual sample location was saved on the BrainLAB workstation, and the corresponding coordinates were transferred offline for subsequent reference. After excision, the tissue samples were immediately bisected: half was snap frozen in liquid nitrogen less than 1 min after removal and stored at –80 °C for ^{1}H HR-MAS spectroscopy; the other half was fixed in 10% zinc formalin, dehydrated by graded ethanols and embedded in Paraplast Plus wax (McCormick Scientific, St. Louis, Missouri, USA) using standardized techniques for pathological analysis.

Histological analysis of the tumor

A pathologist evaluated the slides prepared from tissue samples with hematoxylin and eosin stains to determine the relative contribution of tumor cells to the overall cellularity. A score of '0' denoted neuropil without tumor, '1' indicated an infiltrating tumor margin containing detectable but not abundant numbers of tumor cells, '2' denoted a more cellular infiltrated zone, and '3' denoted highly cellular tumor with relatively few non-neoplastic cells. Tissue samples containing tumor cells (scores > 0) were classified according to WHO standards.

[1]H HR-MAS spectroscopy

Tissue samples weighing between 0.87 and 37.86 mg (median, 9.77 mg) were evaluated. A 35-µL zirconia rotor (custom-designed by Varian,
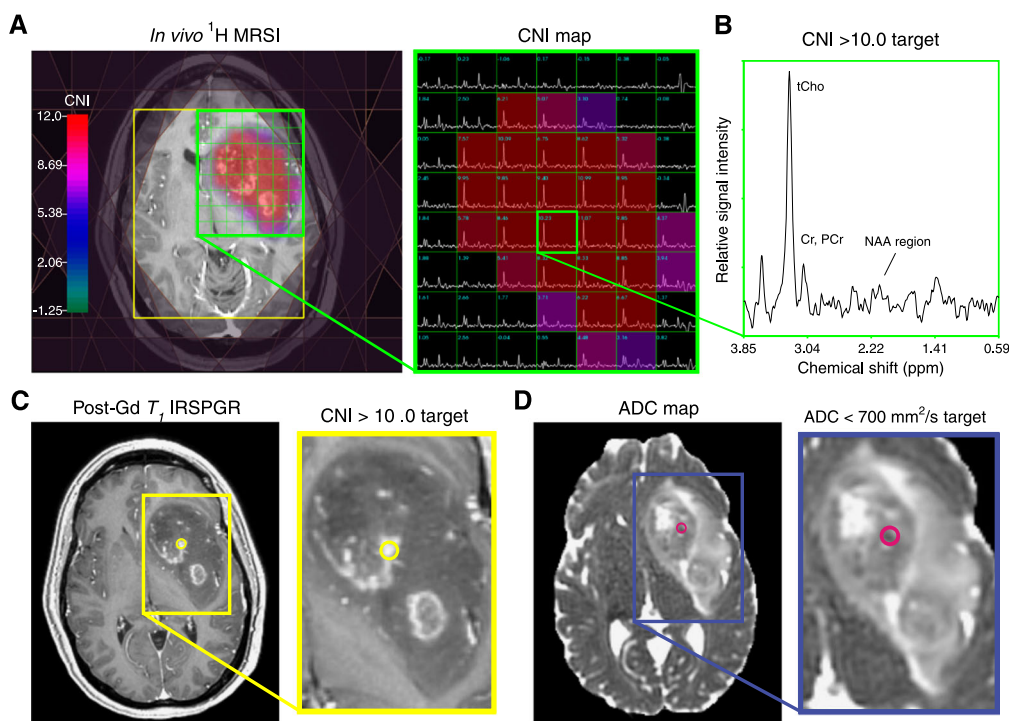

Figure 1. Planning of image- and MRSI-guided tissue sampling. *In vivo* ^{1}H MRS of a patient diagnosed with glioblastoma multiforme. Point-resolved spectroscopic selection (PRESS) coverage defined by yellow box; outer volume suppression (OVS) of lipid shown on periphery; map of the choline to *N*-acetylaspartate (NAA) index (CNI) is overlaid on a T_1-weighted inversion recovery spoiled-gradient echo (IRSPGR) post-Gd image. The corresponding subsets of spectra covering the lesion are shown on the right with CNI values; voxel highlighted in green is designated as a putative tumor region on the basis of elevated CNI within the contrast-enhancing lesion (A). The spectrum from the voxel highlighted in green is enhanced to show the relative metabolite levels contributing to the CNI (B). A 5-mm-diameter target planned for surgical navigation based on this elevated CNI is shown on the T_1-weighted post-contrast image (C). An adjacent target based on restricted diffusion is shown on an apparent diffusion coefficient (ADC) map as a regional hypointensity (D). Cr, creatine; GPC, glycerophosphocholine; PC, phosphocholine; PCr, phosphocreatine; tCho, total choline ([Cho] + [PC] + [GPC]).

Palo Alto, California, USA) was used with 3 μL of 99.9% atom-D deuterium oxide containing 0.75 wt% 3-(trimethylsilyl)propionic acid (Sigma-Aldrich, St. Louis, Missouri, USA) for chemical shift referencing. Data were acquired at 11.7 T at 1 °C with a spin rate of 2250 Hz in a 4-mm gHX nanoprobe with a Varian INOVA 500-MHz multi-nuclear spectrometer. The nanoprobe gHX is an inverse probe, optimized for the direct detection of ^{1}H and the indirect detection of X-nuclei (^{13}C, ^{31}P, ^{15}N), and equipped with a magic angle gradient coil.

A rotor-synchronized, one-dimensional, Carr–Purcell–Meiboom–Gill (CPMG) pulse sequence was run with TR/TE = 4 s/144 ms, 512 scans, 40 000 acquired points, 90° pulse and spectral width of 20 kHz for a total time of 35 min. A relatively long TE was used to maximally suppress the macromolecular background for purposes of metabolite fitting. The electronic reference to access *in vivo* concentrations (ERETIC) method was used to generate an artificial electronic signal that served as an external standard for the estimation of metabolite levels (17).

Pre-processing of the spectra was performed in the time domain using the Java-based Magnetic Resonance User Interface (jMRUI) (18). The estimation of relative one-dimensional metabolite levels was achieved with the semi-parametric algorithm, high-resolution quantum estimation (HR-QUEST), which fits a customized basis set of metabolites to the spectrum (19). The basis set used in this study comprised spectra from 26 metabolite solutions commonly studied in the human brain (Sigma-Aldrich): NAA, free choline (Cho), phosphocholine (PC), glycerophosphocholine (GPC), ethanolamine (Eth), phosphoethanolamine (PE), creatine/phosphocreatine (Cr/PCr), myo-inositol (MI), scyllo-inositol (SI), glucose (Glc), glycine (Gly), total glutathione [tGSH: glutathione (GSH) + glutathione disulfide (GSSG)], glutamate (Glu), glutamine (Gln), 2HG, γ-aminobutyric acid (GABA), taurine (Tau), hypotaurine (hTau), threonine (Thr), acetate (Ace), Lac, alanine (Ala), betaine (Bet), aspartate (Asp), valine (Val) and succinate (Suc). It also included spectra for potential contaminants owing to the surgical sterilization agents methanol (MeOH) and ethanol (EtOH). Each spectrum was evaluated by an experienced spectroscopist to visually assess the goodness of fit, and to determine whether low spectral resolution or signal-to-noise ratio had compromised the evaluation of the metabolite levels. Tissue samples found to have ambiguous or unreliable results were eliminated from subsequent analyses.

Statistical analyses

Tissue samples with tumor scores of 1–3 and metabolite levels with Cramer–Rao error estimates of less than 11% were evaluated. To assess the association of the metabolite parameters with various pathological grades and inter-grade transitions, a proportional odds logistic regression model, adjusted for repeated measures, was applied to evaluate the probability of observing grade outcomes corresponding to different levels of malignancy. This model is written as:

$$logit\left[p\left(Y_{ij} \leq K \mid X_i, Z_i\right)\right] = \alpha_K + X'_{ij}\beta + Z'_{ij}b_i; i = 1, \ldots, N_{subjects};$$

$$K = 1, \ldots, c-1$$

where Y_{ij} is the ordinal outcome for subject i with biopsy measurement j (ranges from 1 to 4), c is the total number of levels of the ordinal variable, X_{ij} is the design matrix for the fixed effects, Z_{ij} is the design matrix for the random effects, α_K are rows corresponding to the jth biopsy specimen, and β and b_i are the vectors of fixed and random parameters. The intercepts are fixed

and category dependent. The odds ratio and p value for each variable are reported. The ordinal-valued outcome mixed effect models were analyzed using PROC GENMOD in SAS (SAS Institute Inc., Cary, North Carolina, USA) v.9.2.

Statistical tests with p values of less than 0.05 were considered to be significant. Metabolites predictive of pathological grade when adjusted for repeated specimen sampling were deemed to be significant predictors and are presented in the results. Because of the exploratory nature of the study, no adjustment for type I error was included.

The second aspect of the analysis concerned the classification of glioma subtypes among relevant groups. Logistic ridge regression models with automatic feature selection were used to determine whether metabolite parameters derived from HR-MAS spectra could jointly predict pathological grades and inter-grade transitions. Classification accuracy was defined as: (number of true positives + number of true negatives)/(sample total). These accuracies were adjusted for multiple tissue samples per patient by repeatedly training the models (100 training sets per model) using only one randomly selected sample per patient, and testing them using the remaining samples. Two feature selection methods were applied. An information gain ratio filtering method was first employed to remove all variables that provided no gain in classification accuracy when evaluated individually, followed by a wrapper-based feature selection method for the evaluation of the worth of subsets of features and selection of the best parsimonious model that was encountered. Average receiver operating characteristic (ROC) curves were generated to visualize the classification performance of each model for the sampled cutoffs, and the average area under the curve (AUC) was calculated.

RESULTS

Summary of analyzed tumor tissue

The numbers of tissue samples that were determined by pathological analysis to contain tumor are summarized according to their grade at initial diagnosis in Table 1. A total of 254 tumor samples acquired from 126 subjects were evaluated using ^{1}H HR-MAS spectroscopy.

Distinguishing metabolite profiles on the basis of primary glioma grade

To be included in the evaluation of profiles from primary grades, samples from recurrent lesions were required to have the same histological grade as that determined at initial diagnosis. As shown in Table 2, 43 of the samples were grade II, 25 grade III and 101 grade IV.

Results from the *ex vivo* ^{1}H HR-MAS spectra were represented in three different ways. Figure 2A–C shows spectra normalized with respect to the area of the ERETIC peak and then averaged to provide a single mean spectrum for each grade. These composite spectra allowed a visual assessment of differences in the relative patterns of the peaks. It should be noted that the relatively high peaks corresponding to Lac were not considered in the comparative analysis as evidence indicates that they cannot reliably reflect *in vivo* levels (20). Figure 2D shows deviations in mean metabolite levels for samples from primary grade III and IV gliomas relative to the levels in primary grade II, with significant increases or decreases in metabolites being highlighted in red and green, respectively. Table 2 provides the

Table 2. Metabolite levels of primary glioma. Relative metabolite levels for each subtype of glioma, displayed as mean ± standard error of the mean (SEM); no units are expressed owing to the T_2 dependence of the Carr–Purcell–Meiboom–Gill (CPMG) acquisition

	Grade II (n = 43)	Grade III (n = 25)	Grade IV (n = 101)	Overall	Grade II versus III	Grade III versus IV	Grade II versus IV
	Mean levels ± SEM			Odds ratios (95% CI)			
	Number of fitted spectral samples			p values			
NAA	29 ± 6 / 17	24 ± 6 / 8	12 ± 2 / 22	0.946 (0.906–0.989) / 0.01	NS	0.927 (0.875–0.981) / 0.009	0.929 (0.873–0.988) / 0.02
Cho	38 ± 7 / 33	64 ± 9 / 21	30 ± 4 / 47	NS	NS	0.979 (0.959–0.999) / 0.04	NS
PC	51 ± 7 / 33	83 ± 15 / 20	67 ± 8 / 29	NS	0.06	NS	NS
tCho	144 ± 19 / 39	183 ± 18 / 23	112 ± 8 / 53	0.996 (0.992–0.999) / 0.02	NS	0.986 (0.984–0.996) / 0.0007	0.08
PE	110 ± 14 / 29	203 ± 31 / 17	132 ± 12 / 47	NS	1.010 (1.003–1.018) / 0.008	NS	NS
(P)Cr	187 ± 23 / 37	166 ± 20 / 23	95 ± 7 / 50	0.991 (0.986–0.995) / <0.0001	NS	0.989 (0.983–0.995) / 0.0001	0.988 (0.981–0.994) / 0.0002
MI	382 ± 44 / 39	321 ± 40 / 23	176 ± 20 / 45	0.995 (0.992–0.999) / 0.04	NS	NS	0.07
Gly	152 ± 23 / 25	269 ± 34 / 20	185 ± 20 / 45	NS	0.08	0.997 (0.994–0.999) / 0.02	NS
tGSH	35 ± 4 / 14	57 ± 20 / 7	61 ± 6 / 47	NS	0.09	NS	1.032 (1.007–1.058) / 0.01
Glu	199 ± 21 / 32	278 ± 43 / 22	296 ± 28 / 57	NS	0.12	NS	0.09
Gln	127 ± 21 / 27	209 ± 35 / 19	149 ± 9 / 50	NS	0.14	0.06	NS
2HG	32 ± 4 / 17	34 ± 4 / 13	0* / 101	0.907 (0.869–0.947) / <0.0001	NS	0.832 (0.753–0.920) / 0.0003	0.827 (0.732–0.935) / 0.002
Thr	39 ± 9 / 16	82 ± 18 / 13	74 ± 12 / 42	NS	0.07	NS	1.019 (1.008–1.003) / 0.02
PC/GPC	111 ± 37 / 31	180 ± 81 / 13	229 ± 31 / 23	NS	0.07	NS	0.02
MCI	325 ± 27 / 38	192 ± 22 / 22	169 ± 14 / 42	0.993 (0.989–0.966) / 0.0002	0.992 (0.986–0.999) / 0.02	NS	0.992 (0.987–0.996) / 0.0005
tCho/(P)Cr	98 ± 13 / 37	124 ± 14 / 21	140 ± 16 / 76	1.007 (1.000–1.013) / 0.04	NS	NS	0.08

2HG, D-2-hydroxyglutarate; Cho, free choline; Cr, creatine; Gln, glutamine; Glu, glutamate; Gly, glycine; GPC, glycerophosphocholine; GSH, glutathione; GSSG, glutathione disulfide; MCI, myo-inositol to total choline index; MI, myo-inositol; NAA, N-acetylaspartate; NS, not significant; PC, phosphocholine; PCr, phosphocreatine; PE, phosphoethanolamine; tCho, total choline ([Cho] + [PC] + [GPC]); tGSH, total glutathione ([GSH] + [GSSG]); Thr, threonine.
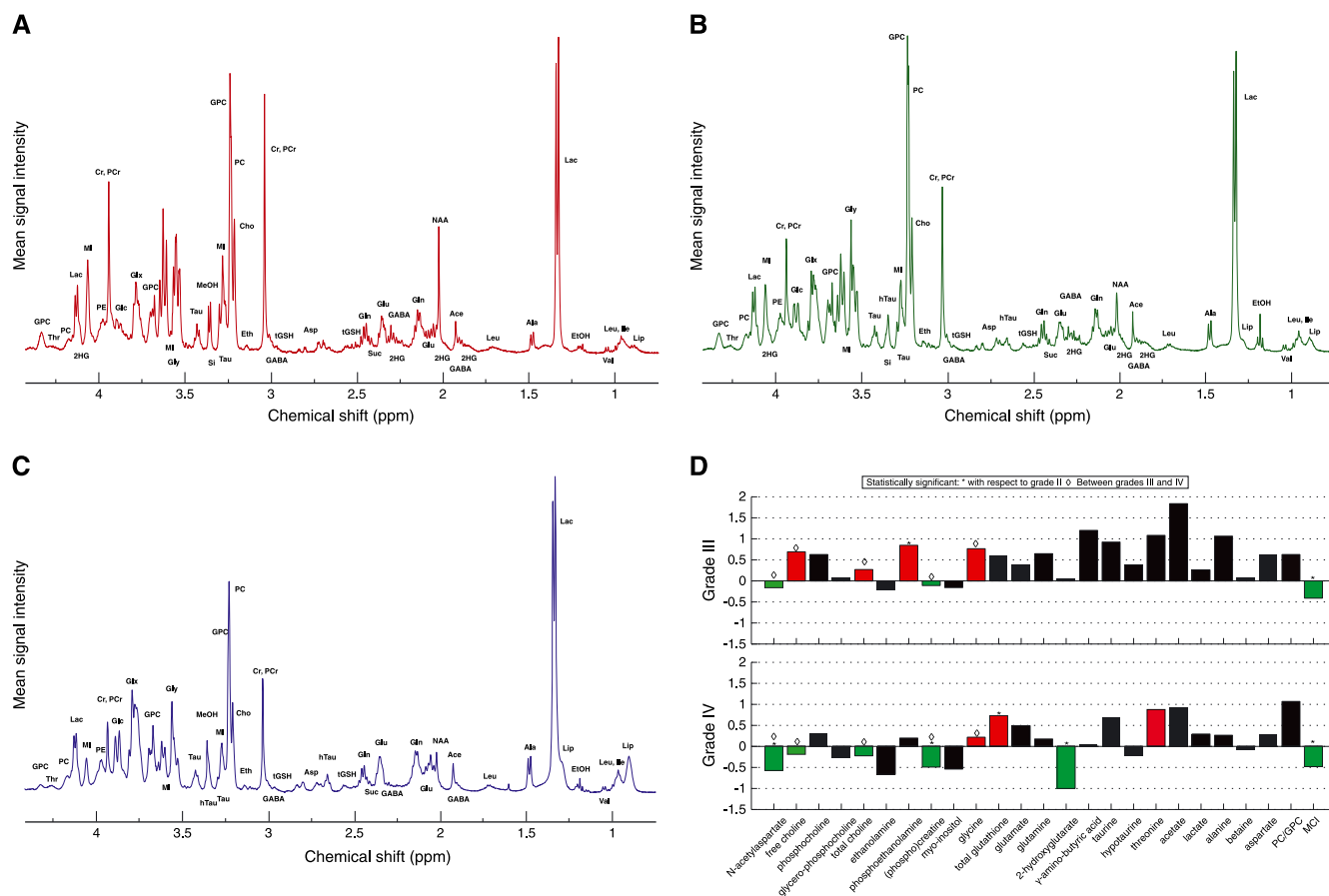*Absence of 2HG resonances confirmed by visual inspection.

Figure 2. Metabolite profiles of primary glioma. Mean Carr–Purcell–Meiboom–Gill (CPMG) spectra for glioma samples histologically defined as grade II ($n = 43$) (A), grade III ($n = 25$) (B) and grade IV glioblastoma multiforme (GBM) ($n = 114$) (C). Deviation in quantified mean metabolite levels of grade II and IV glioma relative to grade II glioma; reported levels are unitless owing to the T_2 dependence of the CPMG acquisition (D). Significant increases or decreases in the metabolite levels displayed as residuals are highlighted in red and green, respectively. Significance was defined as $p < 0.05$ for the comparative analysis among subtypes using the proportional odds logistic regression analysis. MeOH and EtOH are contaminants resulting from surgical sterilization procedures. 2HG, D-2-hydroxyglutarate; Ace, acetate; Ala, alanine; Asp, aspartate; Bet, betaine; Cho, free choline; Cr, PCr, creatine, phosphocreatine; Eth, ethanolamine; EtOH, ethanol; GABA, γ-aminobutyric acid; Glc, glucose; Gln, glutamine; Glu, glutamate; Gly, glycine; GPC, glycerophosphocholine; GSH, glutathione; GSSG, glutathione disulfide; hTau, hypotaurine; Ile, isoleucine; Lac, lactate; Leu, leucine; Lip, lipid; Lys, lysine; MCI, myo-inositol to total choline index; MeOH, methanol; MI, myo-inositol; NAA, N-acetylaspartate; PC, phosphocholine; PE, phosphoethanolamine; SI, scyllo-inositol; Suc, succinate; Tau, taurine; tCho, total choline ([Cho] + [PC] + [GPC]); tGSH, total glutathione ([GSH] + [GSSG]); Thr, threonine; Val, valine.

mean and standard error of individual metabolite levels estimated using HR-QUEST and tested for significant differences between grades.

The mean spectrum for primary grade II gliomas (Fig. 2A) showed prominent peaks corresponding to Cr/PCr, MI, GPC, PC, Cho and NAA, with clear composite peaks corresponding to 2HG, Glu and Gln. The tGSH resonances were relatively low. A key parameter that distinguished primary grade II lesions from the other primary grades (see Table 2) was the ratio of MI to tCho (MCI), which was higher than for both grade III ($p = 0.02$) and grade IV ($p = 0.0005$) lesions. Thr, which is a precursor to both Gly and acetyl-CoA, was either significantly lower or trending towards lower levels in primary grade II relative to primary grade III ($p = 0.07$) and grade IV ($p = 0.02$) lesions.

The mean spectrum from primary grade III glioma showed prominent peaks from GPC, PC and Cho, that were higher relative to Cr/PCr and NAA than for the mean spectrum from grade II glioma (Fig. 2B). There was also a more prominent Gly peak and relatively low peaks from MI. Resonances corresponding to 2HG, Glu and Gln were visible, as well as additional peaks from hTau. The statistical analysis showed that, although there was a general

trend towards higher overall metabolite levels relative to primary grade II lesions (Fig. 2D), only the reduction in MCI ($p = 0.02$) and the increase in PE ($p = 0.008$) reached significance (Table 2).

The mean spectrum from primary grade IV glioma (Fig. 2C) showed relatively lower GPC, Cr/PCr and NAA peaks than both of the lower grades, and lower MI and Gly peaks relative to primary grade III glioma. There were no 2HG resonances seen in individual primary grade IV samples, but relatively more PC relative to GPC, and the presence of Lip peaks at 0.9 and 1.25 ppm that were either lower or absent in grades II and III. Tests of significance showed that the levels of NAA and Cr/PCr were lower than in both grade II ($p = 0.02$ and 0.0002) and grade III ($p = 0.009$ and 0.0001) gliomas. In addition, MCI was significantly lower ($p = 0.0005$) and the level of tGSH higher ($p = 0.01$) than in primary grade II glioma, and the levels of Cho, tCho and Gly were significantly lower than in grade III glioma ($p = 0.04$, 0.0007 and 0.02).

The classification models showed relatively high accuracy in categorizing the metabolite data according to grade (Table 3). There was an 84% accuracy in classifying primary grade II *versus*

Table 3. Glioma classification models. Performance of the machine learning classification schemes, as well as average receiver operating characteristic (ROC) curve areas

	Number of (patients, tissue samples) per grade or transformation	Classification model	Average classification accuracy ± SD (%)	Average ROC curve area
Primary glioma	II (21,43)	II *versus* III	73.1 ± 4.2	0.761
	III (15,25)	III *versus* IV	92.4 ± 2.8	0.960
	IV (50, 101)	II *versus* IV	84.4 ± 3.2	0.869
Recurrent low-grade glioma		$G_{II \to II}$ *versus* $G_{II \to III}$	69.3 ± 4.4	0.746
	$G_{II \to II}$ (21, 43)	$G_{II \to III}$ *versus* $G_{II \to IV}$	72.5 ± 3.1	0.550
	$G_{II \to III}$ (26, 52)	$G_{II \to II}$ *versus* $G_{II \to IV}$	73.6 ± 5.7	0.745
	$G_{II \to IV}$ (8, 19)	$G_{II \to II}$ *versus* TFD	69.9 ± 5.1	0.726
Primary *versus* secondary grade III	$G_{II \to III}$ (26, 52) III (15, 25)	III *versus* $G_{II \to III}$	76.7 ± 5.6	0.676
Primary *versus* secondary GBM	IV (50, 101)	IV *versus* $G_{II \to IV}$	94.4 ± 0.8	0.854
	$G_{II \to IV}$ (8, 19)	IV *versus* $G_{III \to IV}$	95.6 ± 0.9	0.756
	$G_{III \to IV}$ (7, 14)	$G_{II \to IV}$ *versus* $G_{III \to IV}$	61.9 ± 4.1	0.698

GBM, glioblastoma multiforme; TFD, gliomas that have transformed to a higher grade of malignancy.

IV glioma, which underscored the utility of features such as 2HG, tGSH and MCI. Classification of primary grade II *versus* III glioma showed an accuracy of 73%, with the significant differences being in MCI, PE and Gly. Finally, grade III gliomas were separated from glioblastoma multiforme (GBM) with an accuracy of 92% based on higher levels of 2HG, tCho, NAA and Cr/PCr. ROC curves that demonstrate the sensitivity and specificity for these classifications are shown in Fig. 3A.
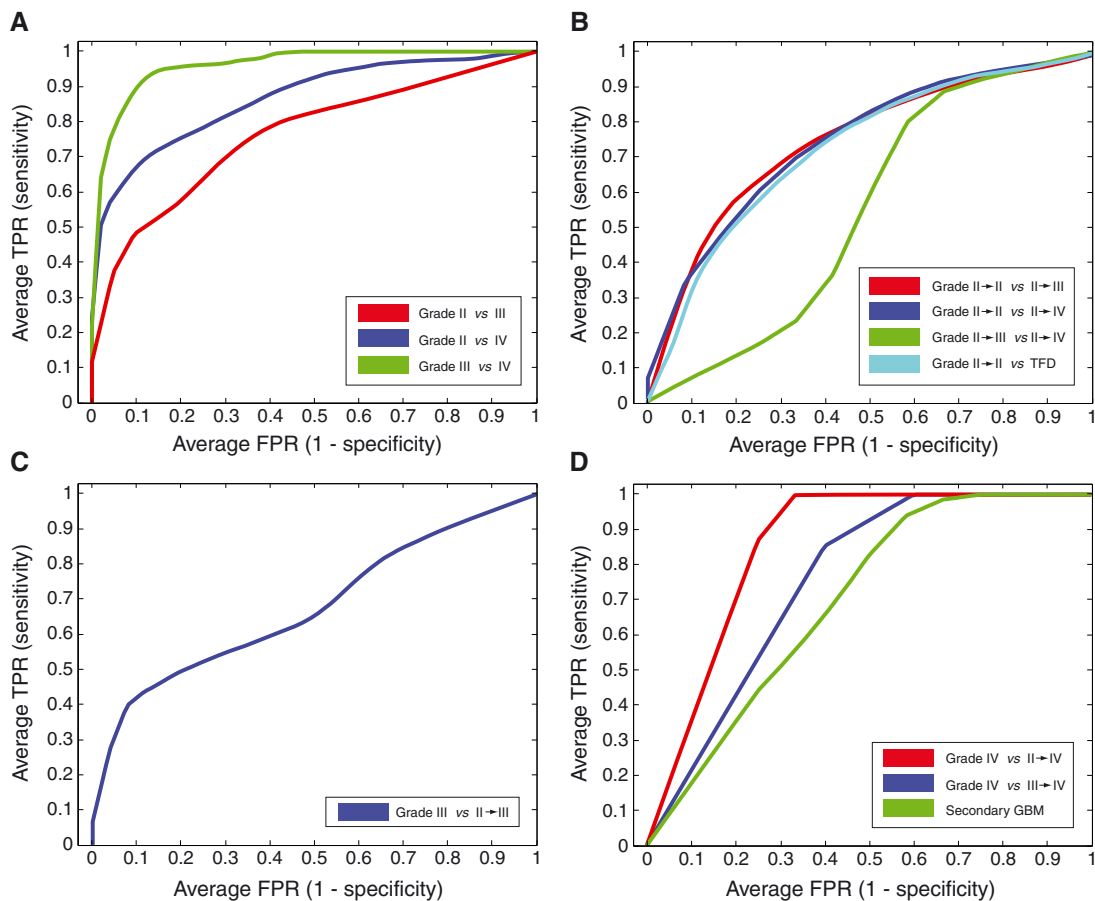
Figure 3. Average receiver operating characteristic (ROC) curves for the logistic ridge regression classification models shown in Table 3: primary glioma (A), recurrent low-grade glioma transformation status (B), primary *versus* secondary grade III (C), and primary *versus* secondary glioblastoma multiforme (GBM) (D). The averaged curves represent the results of 100 training sets per classification model. FPR, false positive rate; TFD, transformed to a higher grade of malignancy; TPR, true positive rate.

Transformation status for recurrent grade II glioma

As can be seen in Table 3, many of the lesions with an original diagnosis of grade II glioma were found to have undergone transformation to a higher pathological grade at recurrence. The largest portion of the tissue samples (46%) showed transformation to grade III ($G_{II \to III}$, $n = 52$) and 16% to grade IV ($G_{II \to IV}$, $n = 19$).

Peaks from the mean spectra (see Fig. 4A–C) corresponding to MI, Cr/PCr and NAA consistently discriminated gliomas that had remained grade II ($G_{II \to II}$) from their transformed counterparts ($G_{II \to III \text{ or } V}$). As was the case for primary glioma samples, there was a transition from GPC to PC as the dominant choline resonance and an increase in the abundance of Lip for grade IV lesions. Figure 4D demonstrates that transformation to higher grade was associated with a progressive increase in metabolite levels. Of particular interest is that the levels of PC ($p = 0.05$ and 0.005) and tGSH ($p = 0.02$ and 0.003) were significantly higher for both transitions, and that 2HG levels were significantly higher for $G_{II \to IV}$ ($p = 0.01$). MCI showed an opposite trend, being lower for both $G_{II \to III}$ ($p = 0.02$) and $G_{II \to IV}$ ($p = 0.002$) relative to $G_{II \to II}$.

The statistical analysis represented in Table 4 emphasizes the significance of these changes.

The statistical models created to discriminate $G_{II \to II}$ versus $G_{II \to III}$ and $G_{II \to III}$ versus $G_{II \to IV}$ demonstrated classification accuracies of 69% and 73%, respectively (Table 3; Fig. 3B). Lower levels of tGSH in $G_{II \to II}$ and elevated levels of PC/GPC in $G_{II \to IV}$ were helpful in distinguishing $G_{II \to III}$. Modeling the optimal classification of $G_{II \to II}$ versus $G_{II \to IV}$ provided an accuracy of 74%, and selected the features of Asp, PC and tGSH as the strongest predictors of $G_{II \to IV}$, whereas high MCI strongly favored $G_{II \to II}$. When comparing all gliomas that had upgraded ($G_{II \to III, IV}$) with those that remained low grade ($G_{II \to II}$), the classification accuracy was 70%.

Primary versus secondary grade III glioma

There were 25 primary grade III (G_{III}) and 52 secondary grade III ($G_{II \to III}$) gliomas. Table 5 indicates that the primary lesions had significantly higher Cho ($p = 0.02$), Gly ($p = 0.03$) and PC/GPC ($p = 0.03$). The classification model of G_{III} versus $G_{II \to III}$ yielded an
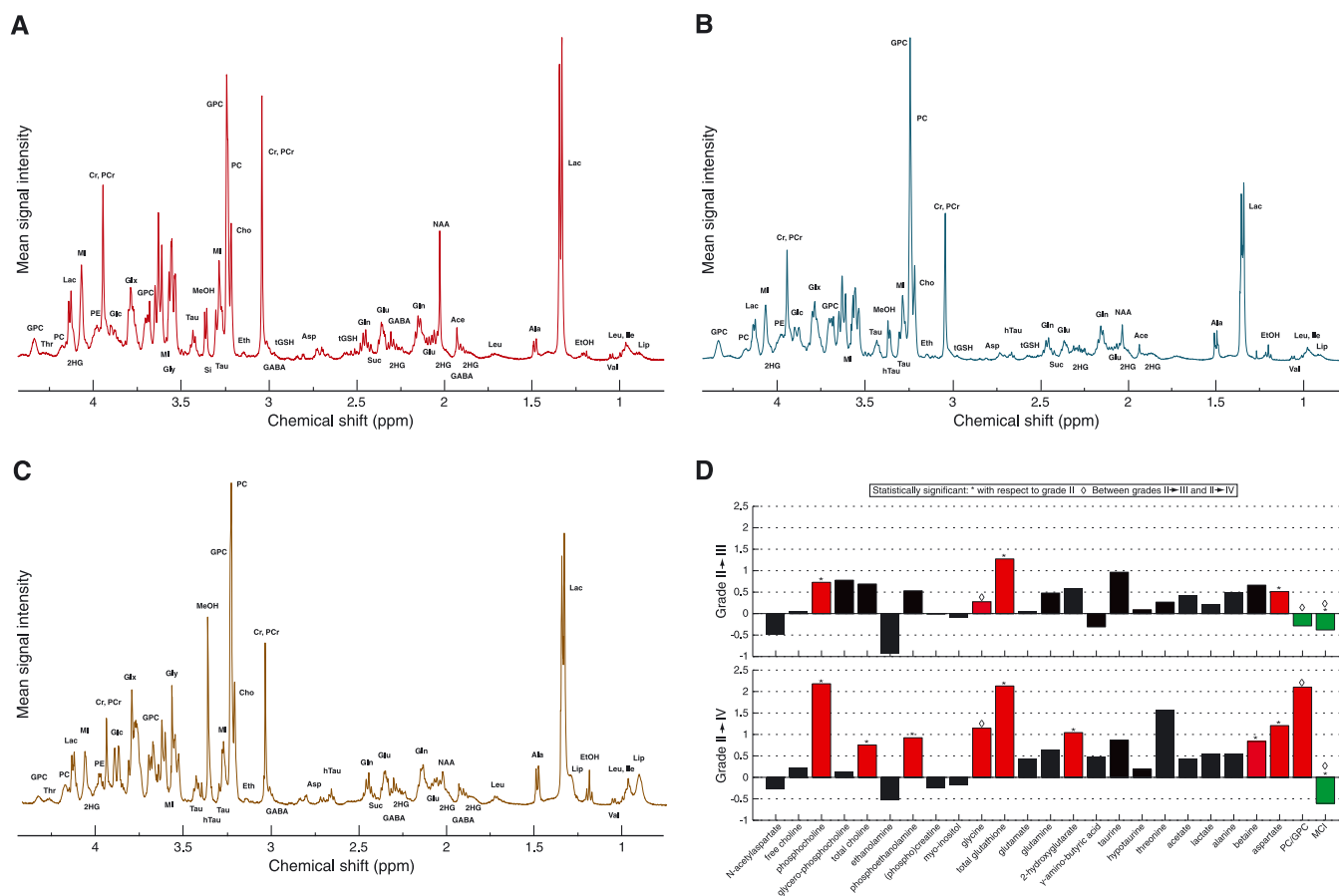
Figure 4. Metabolite profiles of recurrent low-grade glioma. Mean Carr–Purcell–Meiboom–Gill (CPMG) spectra for glioma samples histologically defined according to malignant transformation status as grade II → II ($n = 43$) (A), grade II → III ($n = 52$) (B) and grade II → IV ($n = 19$) (C). Deviation in quantified mean metabolite levels of grade II → III and II → IV glioma relative to grade II → II glioma; reported levels are unitless owing to the T_2 dependence of the CPMG acquisition (D). Significant increases or decreases in the metabolite levels displayed as residuals are highlighted in red and green, respectively. Statistical significance was defined as $p < 0.05$ for the comparative analysis among subtypes using the proportional odds logistic regression analysis. MeOH and EtOH are contaminants resulting from surgical sterilization procedures. 2HG, D-2-hydroxyglutarate; Ace, acetate; Ala, alanine; Asp, aspartate; Bet, betaine; Cho, free choline; Cr, PCr, creatine, phosphocreatine; Eth, ethanolamine; EtOH, ethanol; GABA, γ-aminobutyric acid; Glc, glucose; Gln, glutamine; Glu, glutamate; Gly, glycine; GPC, glycerophosphocholine; GSH, glutathione; GSSG, glutathione disulfide; hTau, hypotaurine; Ile, isoleucine; Lac, lactate; Leu, leucine; Lip, lipid; Lys, lysine; MCI, myo-inositol to total choline index; MeOH, methanol; MI, myo-inositol; NAA, N-acetylaspartate; PC, phosphocholine; PE, phosphoethanolamine; SI, scyllo-inositol; Suc, succinate; Tau, taurine; tCho, total choline ([Cho] + [PC] + [GPC]); tGSH, total glutathione ([GSH] + [GSSG]); Thr, threonine; Val, valine.

Table 4. Metabolite levels of recurrent low-grade glioma. Relative metabolite levels for each subtype of glioma, displayed as mean ± standard error of the mean (SEM); no units are expressed owing to the T_2 dependence of the Carr–Purcell–Meiboom–Gill (CPMG) acquisition

	Grade II → II (n = 43)	Grade II → III (n = 52)	Grade II → IV (n = 19)	Overall	Grade II → II versus II → III	Grade II → II versus II → IV	Grade II → III versus II → IV
	Mean levels ± SEM / Number of fitted spectral samples			Odds ratios (95% CI) / p values			
PC	51 ± 7 / 33	88 ± 12 / 44	162 ± 41 / 14	1.010 (1.003–1.017) / 0.007	1.013 (1.000–1.026) / 0.05	1.018 (1.006–1.031) / 0.005	1.006 (0.999–1.013) / 0.08
tCho	144 ± 19 / 39	243 ± 34 / 52	252 ± 43 / 17	0.06	0.08	1.005 (1.000–1.010) / 0.03	NS
PE	110 ± 14 / 29	168 ± 22 / 41	211 ± 57 / 15	1.003 (1.001–1.006) / 0.02	0.06	1.006 (1.001–1.011) / 0.02	NS
Gly	152 ± 23 / 25	194 ± 20 / 39	327 ± 83 / 13	1.004 (1.001–1.007) / 0.006	NS	0.08	1.004 (1.000–1.007) / 0.05
tGSH	35 ± 0.05 / 14	80 ± 11 / 24	109 ± 20 / 9	1.020 (1.006–1.035) / 0.006	1.056 (1.007–1.108) / 0.02	1.060 (1.020–1.101) / 0.003	NS
2HG	32 ± 5 / 17	51 ± 8 / 33	66 ± 15 / 13	1.012 (1.003–1.022) / 0.009	1.018 (1.001–1.035) / 0.04	1.034 (1.007–1.061) / 0.01	NS
Asp	125 ± 018 / 15	190 ± 23 / 28	277 ± 39 / 11	1.008 (1.002–1.014) / 0.01	1.009 (1.000–1.017) / 0.04	1.017 (1.005–1.030) / 0.007	0.09
PC/GPC	110 ± 37 / 31	79 ± 10 / 42	344 ± 104 / 12	NS	NS	NS	1.014 (1.002–1.026) / 0.02
MCI	325 ± 27 / 38	201 ± 21 / 51	128 ± 13 / 16	0.994 (0.990–0.998) / 0.002	0.995 (0.991–0.999) / 0.02	0.981 (0.970–0.993) / 0.002	0.995 (0.989–1.001) / 0.05
tCho/(P)Cr	98 ± 13 / 37	161 ± 19 / 49	204 ± 34 / 17	1.005 (1.001–1.010) / 0.02	0.06	1.005 (1.000–1.010) / 0.02	NS

2HG, D-2-hydroxyglutarate; Asp, aspartate; Cho, free choline; Cr, creatine; Gly, glycine; GPC, glycerophosphocholine; GSH, glutathione; GSSG, glutathione disulfide; MCI, myo-inositol to total choline index; NS, not significant; PC, phosphocholine; PCr, phosphocreatine; PE, phosphoethanolamine; tCho, total choline ([Cho] + [PC] + [GPC]); tGSH, total glutathione ([GSH] + [GSSG]).

Table 5. Metabolite levels of primary *versus* secondary grade III glioma. Relative metabolite levels for each subtype of glioma, displayed as mean ± standard error of the mean (SEM); no units are expressed owing to the T_2 dependence of the Carr–Purcell–Meiboom–Gill (CPMG) acquisition

	Primary grade III ($n = 25$)	Grade II → III ($n = 52$)	Primary *versus* secondary grade III
	Mean levels ± SEM		Odds ratios (95% CI)
	Number of fitted spectral samples		*p* values
Cho	64 ± 9	40 ± 4	1.021 (1.003–1.039)
	21	48	0.02
NAA	24 ± 6	15 ± 3	1.019 (1.000–1.103)
	8	19	0.05
Gly	269 ± 34	194 ± 20	1.004 (1.001–1.008)
	20	39	0.03
PC/GPC	180 ± 81	79 ± 10	1.004 (1.000–1.008)
	13	42	0.03

Cho, free choline; Gly, glycine; GPC, glycerophosphocholine; NAA, *N*-acetylaspartate; NS, not significant; PC, phosphocholine.
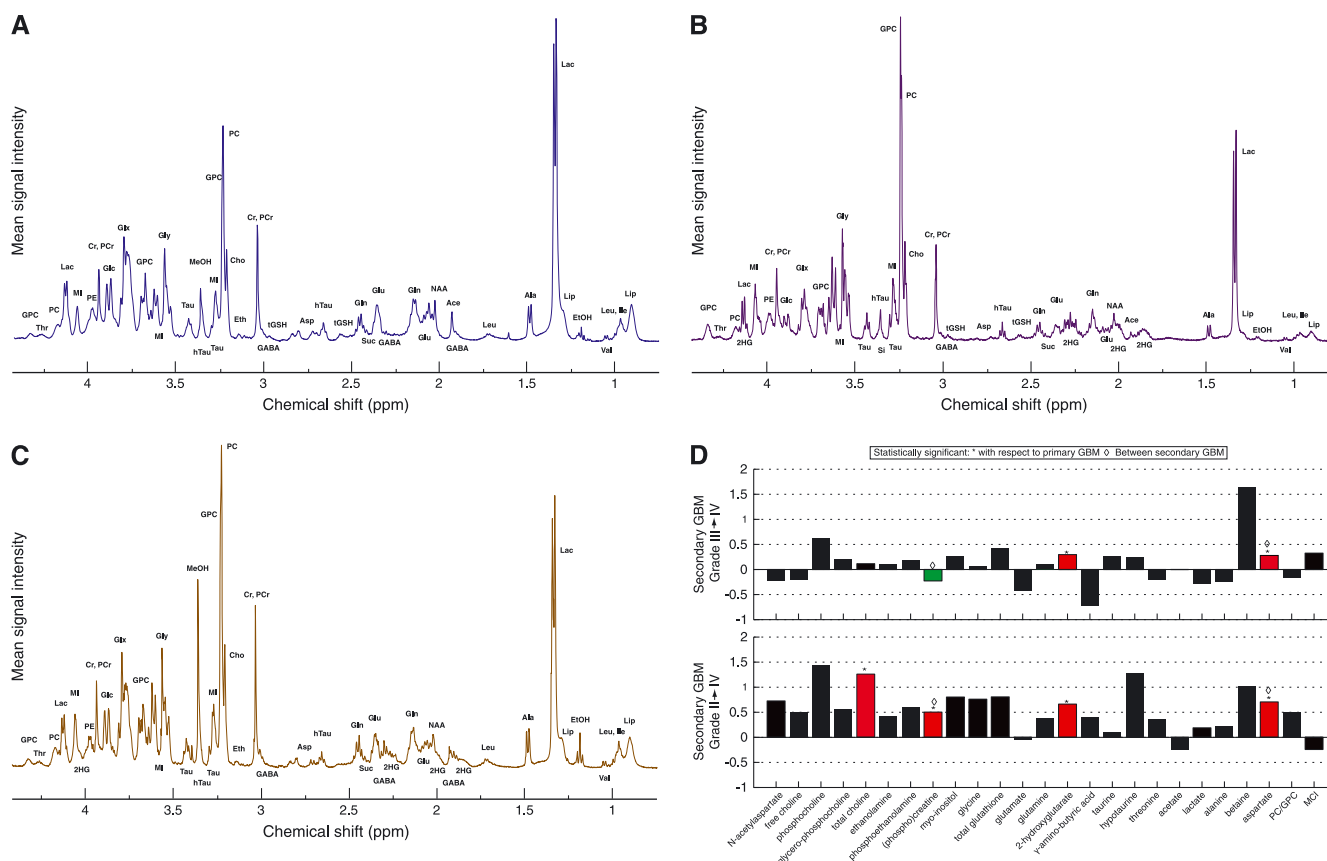

Figure 5. Metabolite profiles of primary *versus* secondary glioblastoma multiforme (GBM). Mean Carr–Purcell–Meiboom–Gill (CPMG) spectra for glioma samples histologically defined as primary grade IV ($n = 101$) (A) and secondary grade III → IV ($n = 14$) (B) or grade II → IV ($n = 19$) (C). Deviation in quantified mean metabolite levels of grade II → III and II → IV glioma relative to grade II → II glioma; reported levels are unitless owing to the T_2 dependence of the CPMG acquisition (D). Significant increases or decreases in the metabolite levels displayed as residuals are highlighted in red and green, respectively. Statistical significance was defined as $p < 0.05$ for the comparative analysis among subtypes using the proportional odds logistic regression analysis. MeOH and EtOH are contaminants resulting from surgical sterilization procedures. 2HG, D-2-hydroxyglutarate; Ace, acetate; Ala, alanine; Asp, aspartate; Bet, betaine; Cho, free choline; Cr, PCr, creatine, phosphocreatine; Eth, ethanolamine; EtOH, ethanol; GABA, γ-aminobutyric acid; Glc, glucose; Gln, glutamine; Glu, glutamate; Gly, glycine; GPC, glycerophosphocholine; GSH, glutathione; GSSG, glutathione disulfide; hTau, hypotaurine; Ile, isoleucine; Lac, lactate; Leu, leucine; Lip, lipid; Lys, lysine; MCI, myo-inositol to total choline index; MeOH, methanol; MI, myo-inositol; NAA, *N*-acetylaspartate; PC, phosphocholine; PE, phosphoethanolamine; SI, scyllo-inositol; Suc, succinate; Tau, taurine; tCho, total choline ([Cho] + [PC] + [GPC]); tGSH, total glutathione ([GSH] + [GSSG]); Thr, threonine; Val, valine.

Table 6. Metabolite levels of primary *versus* secondary glioblastoma multiforme (GBM). Relative metabolite levels for each subtype of glioma, displayed as mean ± standard error of the mean (SEM); no units are expressed owing to the T_2 dependence of the Carr–Purcell–Meiboom–Gill (CPMG) acquisition

	Grade IV (n = 101)	Grade III → IV (n = 14)	Grade II → IV (n = 19)	Overall	Primary GBM versus III → IV	Primary GBM versus II → IV	Grade III → IV versus II → IV
	Mean levels ± SEM			Odds ratios (95% CI)			
	Number of fitted spectral samples			p values			
tCho	112 ± 8	125 ± 27	252 ± 43	0.990 (0.984–0.996)	NS	0.989 (0.981–0.996)	0.10
	53	11	17	0.0004		0.002	
(P)Cr	95 ± 7	73 ± 14	143 ± 22	0.993 (0.987–0.999)	NS	0.992 (0.985–0.998)	0.983 (0.966–1.000)
	50	9	18	0.03		0.01	0.05
2HG	0*	30 ± 3	66 ± 15	0.846 (0.803–0.892)	0.824 (0.747–0.910)	0.830 (0.761–0.905)	0.08
	101	7	13	<0.0001	0.0001	<0.0001	
Asp	162 ± 12	208 ± 34	277 ± 39	0.991 (0.986–0.996)	0.994 (0.990–0.999)	0.991 (0.985–0.996)	NS
	44	6	11	0.001	0.01	0.002	
MI/(P)Cr	208 ± 23	334 ± 61	227 ± 24	NS	0.12	NS	1.010 (1.000–1.019)
	62	6	16				0.04
tCho/(P)Cr	140 ± 16	207 ± 38	204 ± 34	0.995 (0.990–0.999)	0.994 (0.990–0.999)	0.991 (0.985–0.996)	NS
	76	9	17	0.02	0.02	0.03	

2HG, D-2-hydroxyglutarate; Asp, aspartate; Cho, free choline; Cr, creatine; GPC, glycerophosphocholine; MI, myo-inositol; NS, not significant; PC, phosphocholine; PCr, phosphocreatine; tCho, total choline ([Cho] + [PC] + [GPC]).
*Absence of 2HG resonances confirmed by visual inspection.

accuracy of 77%, and indicated that there were relative elevations in GABA, Ala and GPC for primary lesions (Table 3; Fig. 3C).

Primary *versus* secondary GBM

There were 101 samples from primary grade IV and 33 from secondary grade IV ($G_{II \to IV}$, $n = 19$; $G_{III \to IV}$, $n = 14$) glioma. The most obvious differences in the mean spectra (Fig. 5A–C) were the variations in the levels and relative contributions of GPC and PC, the lack of 2HG and the increase in the abundance of Lip. Overall, metabolite levels appeared to be higher in the lesions that arose from grade II glioma (Fig. 5C, D). Statistical analysis indicated that tCho, 2HG and Asp were significantly higher in $G_{II \to IV}$ samples relative to the *de novo* G_{IV} (Fig. 5D and Table 6). Cr/PCr ($p = 0.05$) and MCI ($p = 0.04$) were significantly different for $G_{II \to IV}$ samples. Figure 6 shows spectra from a primary grade IV glioma (red) and a secondary grade IV glioma (blue) that arose from a recurrent grade II lesion. Differences in the portions of spectra corresponding to resonances of 2HG are clearly visible.

The classification models for the discrimination between primary *versus* secondary grade IV glioma were highly accurate (Table 3; Fig. 3D), with the most valuable parameter being the level of 2HG. Accuracies for G_{IV} *versus* $G_{II \to IV}$ and G_{IV} *versus* $G_{III \to IV}$ models were 94% and 96%, respectively. Other parameters, such as tCho and Asp, were found to be useful for distinguishing the G_{IV} *versus* $G_{II \to IV}$ subgroups. The comparison between secondary GBM subtypes ($G_{II \to IV}$ *versus* $G_{III \to IV}$) showed an accuracy of only 62%.

DISCUSSION

This study has provided a characterization of the spectral profiles for infiltrating gliomas. A critical finding was that ^{1}H HR-MAS spectroscopic techniques enabled an accurate classification of these diverse subtypes with respect to standard histological criteria and changes that are associated with malignant transformation at recurrence. This could be important for oncologists in selecting the most appropriate treatment for individual patients in cases in which there is no tissue available from the initial diagnosis. A further critical finding was that several of the *ex vivo* metabolite changes observed could be translated into the *in vivo* setting. These results are of interest for improving the characterization of glioma for non-invasive diagnosis, planning of tissue sampling and surgical resection (21–27).

Table 7 summarizes the important clinical implications of our study according to relevant metabolite findings. A key application of these data is the guidance of tissue sampling at the time of initial diagnosis, given the importance of locating the most malignant region of the tumor for pathological grading. This study suggests that tCho, NAA, Cr/PCr, MI and Lac levels offer the most compelling information for determination of the tumor grade from an *in vivo* perspective. These metabolites are also of particular interest for studying lesion heterogeneity, especially in the case of grade IV glioma, where representative tissue samples may be difficult to obtain at the time of surgical resection. Similar criteria are also proposed in Table 7 for directing tissue sampling with regard to the determination of whether recurrent low-grade gliomas have undergone transformation to a higher grade, and may therefore require more aggressive treatment.

The progressive reduction in MCI for lesions that have transformed from grade II to grade III or IV is a potentially important marker that can be monitored *in vivo* using short-echo ^{1}H MRSI, and may be able to predict transformation to a higher grade or distinguish between recurrent tumor and reactive gliosis (28). Whether other *in vivo* metabolite data can be used
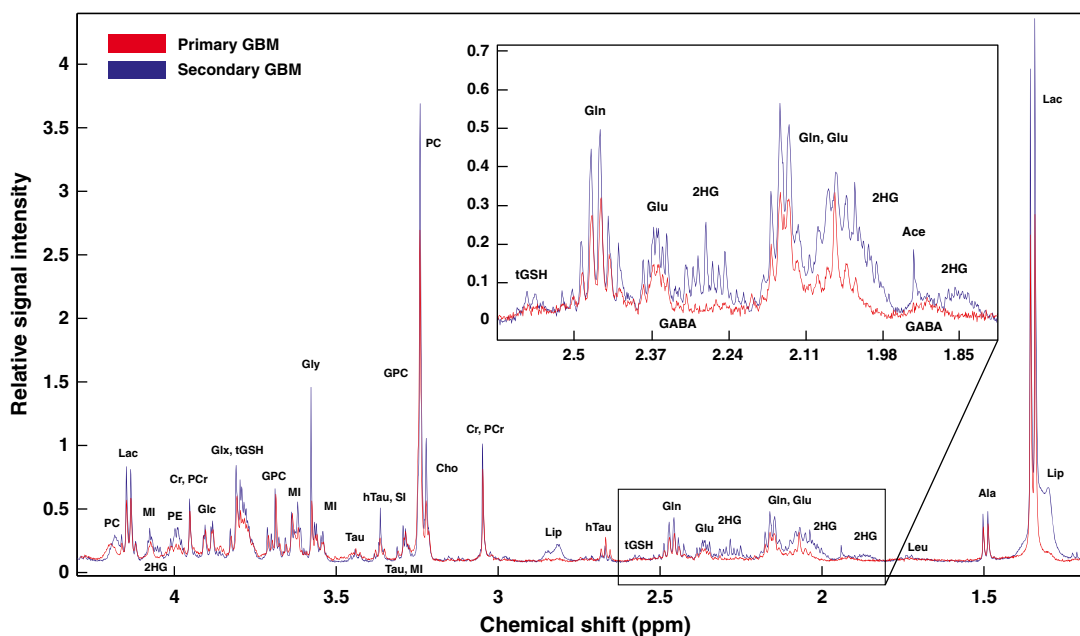

Figure 6. Representative spectra from primary *versus* secondary glioblastoma multiforme (GBM). Red trace represents the high-resolution magic angle spinning (HR-MAS) spectrum from a primary *de novo* GBM; blue trace represent the spectrum from a secondary GBM (grade II → IV). Spectra were normalized by the electronic reference to access in vivo concentrations (ERETIC) signal and tissue sample weights. This example shows the characteristic elevation of metabolites in secondary GBM relative to a primary counterpart, together with the distinguishing presence of the onco-metabolite 2HG. 2HG, D-2-hydroxyglutarate; Ace, acetate; Ala, alanine; Asp, aspartate; Cho, free choline; Cr, PCr, creatine, phosphocreatine; GABA, γ-aminobutyric acid; Glc, glucose; Gln, glutamine; Glu, glutamate; Gly, glycine; GPC, glycerophosphocholine; GSH, glutathione; GSSG, glutathione disulfide; hTau, hypotaurine; Lac, lactate; Lip, lipid; Lys, lysine; MI, myo-inositol; PC, phosphocholine; PE, phosphoethanolamine; SI, scyllo-inositol; Tau, taurine; tGSH, total glutathione ([GSH] + [GSSG]).

Table 7. Summary of relevant clinical implications. Metabolites and indices found to provide potential diagnostic value from this study are summarized according to major clinical needs and challenges

1. Direction of tissue sampling at initial diagnosis

Imaging findings	Major challenge	Metabolite information
Non-enhancing lesion – usually grade II or grade III	To distinguish grade II *versus* grade III (IV)	Elevation of MI/tCho suggests grade II; Target regions with highest tCho, low NAA, low Cr/PCr
Enhancing lesion, no necrosis – usually grade III or grade IV	To distinguish grade III (II) *versus* grade IV	Presence of 2HG implies grade II or III; Target regions with high tCho, low NAA, low Cr/PCr in enhancing region
Enhancing lesion, with necrosis – almost always grade IV	To obtain samples that are representative of tumor properties	Use *in vivo* metabolite data to target regions with different characteristics, i.e. high tCho *versus* low tCho, ±lactate

2. Prediction of malignant transformation

Clinical need	Most relevant metabolite parameters
Targeting most malignant region at surgery	Low MCI, high tCho, low NAA, low Cr/PCr, presence of lactate
Non-invasive assessment of tumor progression	Decrease in MI and increase in tGSH and 2HG imply transformation from grade II to grade III or IV; Elevated PC/GPC implies transformation to grade IV

3. Distinguishing between primary and secondary lesions

Clinical need	Most relevant metabolite parameters
Selection of most appropriate therapy	Elevated 2HG is evidence for a grade IV lesion having arisen from a prior grade II or grade III lesion
Determination of how treatment influences malignant progression	Use temporal changes in tCho, Gly, MCI and PC/GPC to monitor therapy

2HG, D-2-hydroxyglutarate; Cho, free choline; Cr, creatine; Gly, glycine; GPC, glycerophosphocholine; GSH, glutathione; GSSG, glutathione disulfide; MCI, myo-inositol to total choline index; MI, myo-inositol; NAA, *N*-acetylaspartate; PC, phosphocholine; PCr, phosphocreatine; tCho, total choline ([Cho] + [PC] + [GPC]); tGSH, total glutathione ([GSH] + [GSSG]).

to make a non-invasive diagnosis of malignant transformation will depend on the signal-to-noise ratio of the various peaks, the accuracy of the quantitative methods used and the magnitude of the changes that need to be detected. Although *in vivo* detection of tGSH and 2HG has also been reported (9,29–33), these peaks have low signal-to-noise ratios and are located in regions with overlapping spectra from other metabolites. The relative contributions of GPC and PC (4,27,34,35) are a strong *ex vivo* marker for the detection of transformation to grade IV that may relate to specific oncogenic pathways (36), however their contributions to the tCho peak cannot be separated with *in vivo* ^{1}H MRSI. One possibility which may therefore be of interest for future studies of malignant transformation is the use of ultrahigh-field MR scanners to obtain *in vivo* ^{31}P MRSI spectra for assessing changes in PC/GPC.

The third application of this study (Table 7) is to distinguish between primary and secondary lesions, which is especially pertinent for selecting therapy and understanding the diversity of outcomes between patients who were originally thought to have similar pathology. We showed that secondary grade IV gliomas that arise from grade II (Fig. 3C, D) display a very unique profile that is visually characterized by elevations in 2HG, PC, PC/GPC ratio and hTau. The latter metabolite is an intermediate in the biosynthesis of Tau and a sulfur-bearing antioxidant like GSH, capable of reducing reactive oxygen species under conditions of oxidative stress (37,38). A previous HR-MAS study has also indicated that hTau is an important *ex vivo* biomarker for the separation of grade IV glioma and metastatic lesions (39).

The relationship between the levels of 2HG and mutations in the *IDH* genes (*IDH1* and *IDH2*) for up to 70% of lesions diagnosed as grade II glioma has important implications for distinguishing between primary and secondary gliomas (10). Although previous reports in the literature have indicated that 5–12% of primary grade IV gliomas carry *IDH* mutations (10,11,40), none of the tumors that presented as primary grade IV glioma in this study showed detectable levels of 2HG. This discrepancy may be a result of variations in patient populations between institutions and/or the time at which lesions were originally diagnosed. In either case, 2HG remains an important metabolite to monitor *in vivo*.

The evaluation of the genomic properties of primary and secondary grade III gliomas may also help in our understanding of how treatment history influences the processes associated with malignant progression. Although a substantial number of primary grade III glioma samples were found to be *IDH* mutant on the basis of immunohistochemistry, and to have detectable levels of 2HG, there were other differences in their metabolite profile relative to secondary anaplastic glioma, which included significantly lower levels of the tumor markers Gly (41) and PC/GPC. By contrast, transition from primary grade III to secondary grade IV glioma was mainly associated with an increase in tCho. This provides additional motivation for collecting tissue samples in the area of the lesion that is seen to have high tCho from ^{1}H MRSI. Although it was not assessed in this *ex vivo* study, results from *in vivo* measurements of Lac suggest that this metabolite can also identify important targets for directed tissue sampling (42,43).

Despite attempts to optimize the experimental design of this study, there were some inherent limitations that should be noted. The first concerns the possibility of the presence of differences in tumor cellularity between the portions of the samples that were used for histological and metabolite analysis. For this reason, we did not normalize metabolite levels by measures of tumor cellularity, but rather sought to identify robust patterns that were consistent across tumors of similar grade. The second is that the acquisition parameters used for this HR-MAS study meant that the estimated metabolite levels were weighted by their T_2 relaxation times. Despite this T_2 editing, the current literature has not indicated any statistically significant difference in T_2 values between gliomas of different grade (34,44). Moreover, a CMPG sequence was employed with varying TEs to determine whether differences in metabolite T_2 values could be observed between grade II ($n = 3$) and grade IV ($n = 4$) samples, which represent opposite ends of the tumor cellularity spectrum, and no substantial difference was observed for the choline species, Cr/PCr and MI (data not shown).

A third limitation is that the number of samples analyzed in our study did not allow for further stratification on the basis of histological subtypes of low-grade glioma, such as astrocytoma, oligodendroglioma and the mixed oligoastrocytoma (1,2). Previous studies have indicated that there are differences in metabolite parameters among these subtypes (45,46). This may have influenced the accuracy with which we were able to distinguish between lesions that transformed from grade II to grade III *versus* those that remained grade II at recurrence. The fact that there was a higher proportion of lesions with an oligodendroglioma subtype in the population that remained grade II (57.1%) and a smaller proportion of lesions with this subtype in the group that transformed to grade III (36.0%) may explain sources of variance that were not adequately captured in the classification models of this study. Ongoing studies in our institution are collecting a larger number of samples in order to allow for a stratification of lesions by their respective histological subtype, and hence to observe how cellular origin relates to profiles of metabolism.

CONCLUSIONS

The results obtained in this study have elucidated the association between ^{1}H MRSI and the standard histological grading of gliomas that is used clinically for the diagnosis of patients and the determination of appropriate treatments. Metabolite profiles were able to help differentiate between primary glioma subtypes, predict the transformation of recurrent grade II to either grade III or IV, and define the pathological trajectories of primary and secondary glioma of grades III and IV. These novel findings suggest that the discrete metabolomic profiles observed may be related to genomic or epigenomic abnormalities of specific glioma subtypes. Metabolites of significance from *ex vivo* analyses that can readily be observed using clinical MR scanners may also offer *in vivo* biomarkers to clinicians who are attempting to diagnose patients non-invasively and to monitor treatment. The metabolite profiles that have been identified could also help to characterize intra-lesional malignancy in a manner that is not currently addressed by the histopathological grading scheme, and may therefore aid in the delineation of targets for radiation planning and surgical intervention. This is critical for the clinical management of patients with glioma, and provides motivation for future studies that will examine the relationship between ^{1}H MRSI and genetic, epigenetic and biological variations in these lesions.

Acknowledgements

REFERENCES

1. Lois DN, Ohgaki H, Wiestler OD, Cavenee WK, Burger PC, Jouvet A, Scheithauer BW, Kleihues P. The 2007 WHO classification of tumours of the central nervous system. Acta Neuropathol. 2007; 114(2): 97–109.
2. Lopes MBS, VandenBerg SR, Scheithauer BW. The World Health Organization classification of nervous system tumors in experimental neuro-oncology. In Levine AJ, Schmidek HH (eds). *Molecular Genetics of Nervous System Tumors*. Wiley-Liss: New York; 1993, pp. 1–36.
3. Jaeckle KA, Decker PA, Ballman KV, Flynn PJ, Giannini C, Scheithauer BW, Jenkins RB, Bucknew JC. Transformation of low grade glioma and correlation with outcome: an NCCTG database analysis. J. Neurooncol. 2011; 104(1): 253–259.
4. Glunde K, Bhujwalla ZM, Ronen SM. Choline metabolism in malignant transformation. Nat. Rev. Cancer 2011; 11(12): 835–848.
5. Chow LM, Endersby R, Zhu X, Rankin S, Qu C, Zhang J, Broniscer A, Ellison DW, Baker SJ. Cooperativity within and among Pten, p53, Rb pathways induces high-grade astrocytoma in adult brain. Cancer Cell 2011; 19(3): 305–316.
6. Philips HS, Kharbanda S, Chen R, Forrest WF, Sorian RH, Wu TD, Misra A, Nigro JM, Colman H, Soroceanu L, Williams PM, Modrusan Z, Feuerstein BF, Aldape K. Molecular subclasses of high-grade glioma predict prognosis, delineate a pattern of disease progression, and resemble stages in neurogenesis. Cancer Cell 2006; 9(3): 157–173.
7. Verhaak RGW, Hoadley KA, Purdom E, Wang V, Qi Y, Wilkerson MD, Miller CR, Ding L, Golub T, Mesirov JP, Alexe G, Lawrence M, O'Kelly M, Tamayo P, Weir B, Gabriel S, Winckler W, Gupta S, Jakkula L, Feiler HS, Hodgson JG, James CD, Sarkaria JN, Brennen C, Kahn A, Spellman PT, Wilson RK, Speed TP, Gray JW, Meyerson M, Getz G, Perou CM, Hayes DN. The Cancer Genome Atlas Research Network. Integrated genomic analysis identifies clinically relevant subtypes of glioblastoma characterized by abnormalities in PDGFRA, IDH1, EGFR, and NF1. Cancer Cell 2010; 17: 98–110.
8. Elkhaled A, Jalbert LE, Phillips JJ, Yoshihara HAI, Parvataneni R, Srinivasan R, Bourne G, Berger MS, Chang SM, Cha S, Nelson SJ. Magnetic resonance of 2-hydroxyglutarate in IDH1-mutated low-grade gliomas. Sci. Transl. Med. 2012; 4: 116ra5.
9. Andronesi OC, Kim GS, Gerstner E, Batchelor T, Tzika AA, Fantin VR, Vander Heiden MG, Sorenson GS. Detection of 2-hydroxyglutarate in IDH-mutated glioma patients by in vivo spectral-editing and 2D correlation magnetic resonance spectroscopy. Sci. Transl. Med. 2012; 4: 116ra4.
10. Yan H, Parsons DW, Jin G, McLendon R, Rasheed BA, Yuan W, Kos I, Batinic-Haberle I, Jones S, Riggins GJ, Friedman H, Friedman A, Reardon D, Herndon J, Kinzler KW, Velculescu VE, Vogelstein B, Bigner DD. *IDH1* and *IDH2* mutations in gliomas. N. Engl. J. Med. 2009; 360: 765–773.
11. Parsons DW, Jones S, Zhang X, Lin JC, Leary RJ, Angenendt P, Mankoo P, Carter H, Siu I, Gallia GL, Olivi A, McLendon R, Rasheed BA, Keir S, Nikolskaya T, Nikolsky Y, Busam D, Tekleab H, Diaz LA Jr, Hartigan J, Smith DR, Strausberg RL, Marie SKN, Shinjo SMO, Yan H, Riggins GJ, Bigner DD, Karchin R, Papadopoulos N, Parmigiani G, Vogelstein B, Velculescu VE, Kinzler KW. An integrated genomic analysis of human glioblastoma multiforme. Science 2008; 321: 1807–1812.
12. Houillier C, Wang X, Kaloshi G, Mokhtari K, Guillevin R, Laffaire J, Paris S, Boisselier B, Idbaih A, Laigle-Donadey F, Hoang-Xuan K, Sanson M, Delattre JY. *IDH1* or *IDH2* mutations predict longer survival and response to temozolomide in low-grade gliomas. Neurology 2010; 75: 1560–1566.
13. Hartmann C, Hentschel B, Wick W, Capper D, Felsberg J, Simon M, Westphal M, Schackert G, Meyermann R, Pietsch T, Reifenberger G, Weller M, Loeffler M, von Deimling A. Patients with *IDH1* wild type anaplastic astrocytomas exhibit worse prognosis than IDH1-mutated glioblastomas, and *IDH1* mutation status accounts for the unfavorable prognostic effect of higher age: implications for classification of gliomas. Acta Neuropathol. 2010; 120: 707–718.
14. Park I, Chen AP, Zierhut M, Ozturk-Isik E, Vigneron DB, Nelson SJ. Implementation of 3T lactate-edited 3D ^{1}H MR spectroscopic imaging with flyback echo-planar readout for glioma patients. Ann. Biomed. Eng. 2011; 39: 193–204.
15. Basser PJ, Pierpaoli C. Microstructural and physiological features of tissues elucidated by quantitative diffusion-tensor MRI. J. Magn. Reson. B, 1996; 111: 209–219.
16. McKnight TR, Noworolski SM, Vigneron DB, Nelson SJ. An automated technique for the quantitative assessment of 3D-MRSI data from patients with glioma. J. Magn. Reson. Imaging 2001; 13: 167–177.
17. Albers MJ, Butler TN, Rahwa I, Bao N, Keshari KR, Swanson MG, Kurhanewicz, J. Evaluation of the ERETIC method as an improved quantitative reference for ^{1}H HR-MAS spectroscopy of prostate tissue. Magn. Reson. Med. 2009; 61: 525–532.
18. Stefan D, Cesare FD, Andrasescu A, Popa E, Lazariev A, Vescovo E, Strbak O, Williams S, Starcuk Z, Cabanas M, van Ormondt D, Graveron-Demily D. Quantitation of magnetic resonance spectroscopy signals: the jMRUI software package. Meas. Sci. Technol. 2009; 20: 104035(9pp).
19. Ratiney H, Albers MJ, Rabeson H, Kurhanewicz J. Semi-parametric time-domain quantification of HR-MAS data from prostate tissue. NMR Biomed. 2010; 23: 1–13.
20. Opstad KS, Bell BA, Griffiths JR, Howe FA. An assessment of the effects of sample ischaemia and spinning time on the metabolic profile of brain tumour biopsy specimens as determined by high-resolution magic angle spinning ^{1}H NMR. NMR Biomed. 2008; 21(10): 1138–1147.
21. Opstad KS, Wright AJ, Bell A, Griffiths JR, Howe FA. Correlations between in vivo ^{1}H MRS and ex vivo ^{1}H HR-MAS metabolite measurements in adult human gliomas. J. Magn. Reson. Imaging 2010; 31: 289–297.
22. Constantin A, Elkhaled A, Jalbert L, Srinivasan R, Cha S, Chang SM, Bajcsy R, Nelson SJ. Identifying malignant transformations in recurrent low grade gliomas using high resolution magic angle spinning spectroscopy. Artif. Intell. Med. 2012; 55(1): 61–70.
23. Vettukattil R, Gulati M, Sjobakk TE, Jakola AS, Kvernmo NA, Torp SH, Bathen TF, Gulati S, Gribbestad IS. Differentiating diffuse World Health Organization grade II and IV astrocytomas with ex vivo magnetic resonance spectroscopy. Neurosurgery 2013; 72(2): 186–195.
24. Sjobakk TE, Vettukattil R, Gulati M, Gulati S, Lundgren S, Gribbestad IS, Torp SH, Bathen TF. Metabolic profiles of brain metastases. Int. J. Mol. Sci. 2013; 14(1): 2104–2118.
25. Martinez-Bisbal MC, Marti-Bonmati L, Piquer J, Revert A, Ferrer P, Llacer JL, Piotto M, Assemat O, Celda B. ^{1}H and ^{13}C HR-MAS spectroscopy of intact biopsy samples ex vivo and in vivo ^{1}H MRS study of human high grade gliomas. NMR Biomed. 2004; 17(4): 191–205.
26. Rutter A, Hugenholtz H, Saunders JK, Smith IC. Classification of brain tumors by ex vivo ^{1}H NMR spectroscopy. J. Neurochem. 1995; 64(4): 1655–1661.
27. Righi V, Roda JM, Paz J, Mucci A, Tugnoli V, Rodriguez-Tarduchy G, Barrios L, Schenetti L, Cerdan S, Garcia-Martin ML. ^{1}H HR-MAS and genomic analysis of human tumor biopsies discriminate between high and low grade astrocytomas. NMR Biomed. 2009; 22: 629–637.
28. Srinivasan R, Phillips JJ, Vandenberg SR, Polley MY, Bourne G, Au A, Pirzkall A, Cha S, Chang SM, Nelson SJ. Ex vivo MR spectroscopic measure differentiates tumor from treatment effects in GBM. Neuro-Oncol. 2010; 12: 1152–1161.
29. Opstad KS, Provencher SW, Bell BA, Griffiths JR, Howe FA. Detection of elevated glutathione in meningiomas by quantitative in vivo ^{1}H MRS. Magn. Reson. Med. 2003; 49: 632–637.
30. Thelwal PE, Yemin AY, Gillian TL, Simpson NE, Kasibhatla MS, Rabbani ZN, MacDonald JM, Blackband SJ, Gamcsik MP. Noninvasive in vivo detection of glutathione metabolism in tumors. Cancer Res. 2005; 65: 10149–10153.
31. Srinivasan R, Ratiney H, Hammond-Rosenbluth KE, Pelletier D, Nelson SJ. MR spectroscopic imaging of glutathione in the white and gray matter at 7 T with an application to multiple sclerosis. Magn. Reson. Imaging 2010; 28(2): 163–170.
32. Choi C, Ganji SK, DeBerardinis RJ, Rakheja D, Kovacs Z, Yang XL, Mashimo T, Taisanen J, Marin-Valencia I, Pascual JM, Madden CJ, Mickey BE, Malloy CR, Bachoo RM, Maher EA. 2-Hydroxyglutarate detection by magnetic resonance spectroscopy in IDH-mutated patients with gliomas. Nat. Med. 2012; 18(4): 624–629.

33. Pope WB, Prins RM, Albert Thomas M, Nagarajan R, Yen KE, Bittinger MA, Salamon N, Chou AP, Yong WH, Soto H, Wilson N, Driggers E, Jang HG, Su SM, Schenkein DP, Lai A, Cloughesy TF, Kornblum HI, Wu H, Fantin VR, Liau LM. Non-invasive detection of 2-hydroxyglutarate and other metabolites in IDH1 mutant glioma patients using magnetic resonance spectroscopy. J. Neurooncol. 2012; 107(1): 197–205.

34. Usenius JP, Vainio P, Hernesniemi J, Kauppinen RA. Choline-containing compounds in human astrocytomas studied by ^{1}H NMR spectroscopy in vivo and in vitro. J. Neurochem. 1994; 63(4): 1538–1543.

35. Podo F. Tumour phospholipid metabolism. NMR Biomed. 1999; 12: 413–439.

36. Venkatesh HS, Chaumeil MM, Ward CS, Haas-Kogan DA, James CD, Ronen SM. Reduced phosphocholine and hyperpolarized lactate provide magnetic resonance biomarkers of PI3K/Akt/mTOR inhibition in glioblastoma. Neuro-Oncol. 2012; 14(3): 315–325.

37. Aruoma OI, Halliwell B, Hoey BM, Butler J. The antioxidant action of taurine, hypotaurine and their metabolic precursor. Biochem. J. 1988; 256(1): 251–255.

38. Brand A, Leibfritz D, Hamprecht B, Dringen R. Metabolism of cysteine in astroglial cells: synthesis of hypotaurine and taurine. J. Neurochem. 1998; 71: 827–832.

39. Wright AJ, Fellows GA, Griffiths JR, Wilson M, Bell BA, Howe FA. Ex vivo HRMAS of adult brain tumours: metabolite quantification and assignment of tumour biomarkers. Molec. Cancer, 2010; 9: 66.

40. Presner JR, Chinaiyan AM. Metabolism unhinged: IDH mutations in cancer. Nat. Med. 2011; 17: 291–293.

41. Righi V, Andronesi OC, Mintzopoulos D, Black PM, Tzika AA. High-resolution magic angle spinning magnetic resonance spectroscopy detects glycine as a biomarker in brain tumors. Int. J. Oncol. 2010; 36(2): 301–306.

42. Chang SM, Nelson SJ, Vandenberg S, Cha S, Prados M, Butowski N, McDermott M, Parsa AT, Aghi M, Clarke J, Berger M. Integration of preoperative anatomic and metabolic physiologic imaging of newly diagnosed glioma. J. Neurooncol. 2009; 92(3): 401–415.

43. Saraswathy S, Crawford FW, Lamborn KR, Pirzkall A, Chang S, Cha S, Nelson SJ. Evaluation of MR markers that predict survival in patients with newly diagnosed GBM prior to adjuvant therapy. J. Neurooncol. 2009; 91(1): 69–81.

44. Li Y, Srinivasan R, Ratiney H, Lu Y, Chang SM, Nelson SJ. Comparison of T_1 and T_2 metabolite relaxation times in glioma and normal brain at 3T. J. Magn. Reson. Imaging 2008; 28(2): 342–350.

45. Chawla S, Oleaga L, Wang S, Krejza J, Woo JH, O'Rourke DM, Judy KD, Grady MS, Melhem ER, Poptani H. Role of proton magnetic resonance spectroscopy in differentiating oligodendrogliomas and astrocytomas. J. Neuroimaging 2010; 20(1): 3–8.

46. Huang J, Gholami B, Agar NYR, Norton I, Haddad WM, Tannenbaum AR. Classification of astrocytomas and oligodendrogliomas from mass spectrometry data using sparse kernel machines. *Engineering in Medicine and Biology Society, EMBC, Annual International Conference of the IEEE*, Boston, Massachusetts, USA, 2011; 7965–7968.